



INDC(NDS)-0660
Distr. IBA

INDC International Nuclear Data Committee

Developments in the Ion Beam Analysis Nuclear Data Library (IBANDL)

Editor P. Dimitriou

June 2014

Selected INDC documents may be downloaded in electronic form from
<http://www-nds.iaea.org/publications>
or sent as an e-mail attachment.

Requests for hardcopy or e-mail transmittal should be directed to
NDS.Contact-Point@iaea.org

or to:

Nuclear Data Section
International Atomic Energy Agency
Vienna International Centre
PO Box 100
1400 Vienna
Austria

Printed by the IAEA in Austria

June 2014

**Developments in the Ion Beam Analysis Nuclear Data Library
(IBANDL)**

Editor P. Dimitriou

Developments in the Ion Beam Analysis Data Library (IBANDL) regarding data updates and new evaluations of light-particle elastic scattering and gamma-ray emitting reactions are presented.

Based on the work performed by Alexander Gurbich, Institute of Physics and Power Engineering, Obninsk, Russian Federation, according to a Contractual Service Agreement with the IAEA Nuclear Data Section.

June 2014

TABLE OF CONTENTS

Contents

1. Objectives.....	7
2. Implementation	7
2.1. Addition of new data sets to IBANDL.....	7
2.2. IBANDL/SigmaCalc development	12
2.3. Evaluation of charged particle reaction cross sections.....	16
2.3.1. The $^{12}\text{C}(d,p_0)^{13}\text{C}$ cross section.....	16
2.3.2. The $^{28}\text{Si}(\alpha,\alpha_0)^{28}\text{Si}$ and $^{\text{nat}}\text{Si}(\alpha,\alpha_0)^{\text{nat}}\text{Si}$ cross sections	22
2.3.3. The $^{13}\text{C}(p,p_0)^{13}\text{C}$ cross section.....	25
2.4. Evaluation for PIGE	28
2.4.1. The $^{23}\text{Na}(p,p_1\gamma)^{23}\text{Na}$ cross section	28
2.4.2. The $^{27}\text{Al}(p,p_1\gamma)^{27}\text{Al}$ cross section.....	31
2.4.3. The $^{52}\text{Cr}(p,\gamma)^{53}\text{Mn}$ cross section.....	33
3. Conclusions	35
References	37

1. Objectives

The objectives of this work performed under an IAEA Nuclear Data Section (IAEA NDS) Contractual Service Agreement (CSA) were as follows:

- continuous support of the IBANDL database including improvements in the internal structure of the database and addition of new data sets taken from the literature and/or supplied by authors;
- maintenance and development of the SigmaCalc web site;
- evaluation of the differential cross sections for elastic scattering of light particles;
- inclusion in IBANDL of data for Particle Induced Gamma-ray Emission (PIGE);
- development of an evaluation methodology for PIGE data.

2. Implementation

2.1. Addition of new data sets to IBANDL

The content of IBANDL was updated by first searching for data available in the EXFOR database. An automatized procedure implemented by V. Zerkin (IAEA NDS) creates R33 buttons for EXFOR data that could be of potential relevance to IBANDL. A careful inspection of those EXFOR files supplied with a R33 button was performed to identify those which were indeed suitable for Ion Beam Analysis. Additionally, a search for relevant data was made in the literature. The search was focused mainly on the PIGE data however, a significant number of EBS and NRA data were also found. In addition some mistakes were found and corrected in the existing R33 files. The cumulative inventory of updates is presented in Table 1 and a list of references sent to NDS for digitizing is given in Table 2.

Table 1. The updates of IBANDL with files submitted to NDS.

Date	Cross section	Source	Comments
17.10.13	$^{18}\text{O}(\alpha, \alpha_0)^{18}\text{O}$	Journal de Physique, Vol.29, p.271 (1968)	EXFOR:D0272002
17.10.13	$^{18}\text{O}(p, p_0)^{18}\text{O}$	Physical Review, Part C, Nuclear Physics, Vol.69, p.024602 (2004)	EXFOR: D0352002, D0352003
17.10.13	$^{18}\text{O}(p, p_0)^{18}\text{O}$	Annals of Physics (New York), Vol.51, Issue.3, p.461 (1969)	EXFOR:C1918002,
03.10.13	$^{12}\text{C}(^3\text{He}, p_0)^{14}\text{N}$	R.L. Johnston et al. Physical Review v.109 (1958) 884	A. Gurbich: data in file c2hp0i.r33 deleted
30.09.13	$^{16}\text{O}(\alpha, \alpha_0)^{16}\text{O}$	J.R. Cameron, Phys. Rev. 90 (1953) 839	A. Gurbich: file o6aa0h.r33 deleted

18.09.13	$^{15}\text{N}(\alpha, \alpha_0) ^{15}\text{N}$	S. Wilmes+(2002), Jour. Physical Review, Part C, Vol.66, p.065802	EXFOR: F0748002
18.09.13	$^{14}\text{N}(p, p_0) ^{14}\text{N}$	M.L. West+(1969), Jour. Physical Review, Vol.179, p.1047	EXFOR: C1513002
18.09.13	$^{56}\text{Fe}(p, p\gamma_{1-0}) ^{56}\text{Fe}$	G.A. Krivonosov+(1976), Jour. Yadernaya Fizika, Vol.24, p.461	EXFOR: F0920010
16.09.13	$^{107}\text{Ag}(p, p\gamma_{3-0}) ^{107}\text{Ag}$ $^{107}\text{Ag}(p, p\gamma_{4-0}) ^{107}\text{Ag}$ $^{109}\text{Ag}(p, p\gamma_{3-0}) ^{109}\text{Ag}$ $^{109}\text{Ag}(p, p\gamma_{4-0}) ^{109}\text{Ag}$ $^{197}\text{Au}(p, p\gamma_{2-1}) ^{197}\text{Au}$ $^{197}\text{Au}(p, p\gamma_{3-0}) ^{197}\text{Au}$ $^{110}\text{Pd}(p, p\gamma_{1-0}) ^{110}\text{Pd}$ $^{104}\text{Pd}(p, p\gamma_{1-0}) ^{104}\text{Pd}$ $^{108}\text{Pd}(p, p\gamma_{1-0}) ^{108}\text{Pd}$ $^{194}\text{Pt}(p, p\gamma_{1-0}) ^{194}\text{Pt}$ $^{195}\text{Pt}(p, p\gamma_{1-0}) ^{195}\text{Pt}$ $^{195}\text{Pt}(p, p\gamma_{4-0}) ^{195}\text{Pt}$ $^{195}\text{Pt}(p, p\gamma_{6-0}) ^{195}\text{Pt}$ $^{196}\text{Pt}(p, p\gamma_{1-0}) ^{196}\text{Pt}$ $^{198}\text{Pt}(p, p\gamma_{1-0}) ^{198}\text{Pt}$ $^{103}\text{Rh}(p, p\gamma_{3-0}) ^{103}\text{Rh}$ $^{103}\text{Rh}(p, p\gamma_{4-0}) ^{103}\text{Rh}$	G. Deconninck+, J. Radioanal. Chem. 24 (1975) 437	Gurbich
20.08.13	$^7\text{Li}(p, p\gamma_{1-0}) ^7\text{Li}$	B.Ja. Guzhovskij+(1984), Jour. Izv.Kaz.Akad.Nauk,Ser.Fiz.-Mat., Vol.4, p.24	EXFOR: F0024002
20.08.13	$^{16}\text{O}(d, p_1) ^{17}\text{O}$	H.C. Kim+(1964), Jour. Nuclear Physics, Vol.57, p.526	Correction of the file o6dp1o.r33 requested by A. Gurbich, EXFOR: C1438002
14.08.13	$^{52}\text{Cr}(p, \gamma) ^{53}\text{Mn}$ $^{54}\text{Fe}(p, \gamma) ^{55}\text{Co}$	S.R. Kennett et. al. NP/A,363,233,1981	EXFOR: D0682002 EXFOR: D0682004
19.07.13	$^{32}\text{S}(p, p_0) ^{32}\text{S}$	A. Li-Scholz et al. Appl. Phys. Lett. 56 (1990) 2696	Gurbich
19.07.13	$^{23}\text{Na}(p, \alpha\gamma_{1-0}) ^{20}\text{Ne}$ $^{23}\text{Na}(p, p\gamma_{1-0}) ^{23}\text{Na}$	P. Trocellier, Ch. Engelmann. J. Radioanal. Chem. 67 (1981) 135	Gurbich
28.06.13	$^{32}\text{S}(\alpha, \alpha_0) ^{32}\text{S}$	A. Coban+(1999), Jour. Nuclear Physics, Section A, Vol.645, p.3	EXFOR: O0963002
28.06.13	$^{16}\text{O}(d, p_0) ^{16}\text{O}$	V. Gomes+(1965), Jour. Nuclear Physics,	EXFOR: D0323003

		Vol.68, p.417	
28.06.13	$^{16}\text{O}(d,\alpha_1)^{14}\text{N}$	O. Dietzsch+(1968), Jour. Nuclear Physics, Section A, Vol.114, p.330	EXFOR: F0727006
28.06.13	$^{12}\text{C}(d,p_1)^{13}\text{C}$	M. Lambert+(1966), Jour. Comptes Rendus, Serie B, Physique, Vol.262, p.1459	EXFOR: D0679004
20.06.13	$^{16}\text{O}(d,p_0)^{17}\text{O}$	H.C. Kim+(1964), Jour. Nuclear Physics, Vol.57, p.526	EXFOR: C1438002
20.06.13	$^{14}\text{N}(d,p\gamma_{7-0})^{15}\text{N}$ $^{14}\text{N}(d,p\gamma_{5-0})^{15}\text{N}$	H. Van Bebber + Nucl. Instr. & Meth. B136-138 (1998) 72	EXFOR: O0856000 EXFOR: O0856000
20.06.13	$^6\text{Li}(\alpha,d_0)^8\text{Be}$	H.R. Blieden+(1963), Jour. Nuclear Physics, Vol.49, p.209	EXFOR: F0167013
20.06.13	$^{19}\text{F}(p,\alpha\gamma_{4-0})^{16}\text{O}$ $^{19}\text{F}(p,\alpha\gamma_{3-0})^{16}\text{O}$ $^{19}\text{F}(p,\alpha\gamma_{2-0})^{16}\text{O}$ $^{19}\text{F}(p,\alpha\gamma_{2-0+3-0+4-0})^{16}\text{O}$	A. Fessler et al., NIM A450 (2000) 353	Gurbich
20.06.13	$^{19}\text{F}(p,\alpha\gamma_{2-0+3-0+4-0})^{16}\text{O}$ $^{19}\text{F}(p,\alpha\gamma_{4-0})^{16}\text{O}$ $^{19}\text{F}(p,\alpha\gamma_{3-0})^{16}\text{O}$ $^{19}\text{F}(p,\alpha\gamma_{2-0})^{16}\text{O}$ $^{19}\text{F}(p,p\gamma_{2-0})^{19}\text{F}$ $^{19}\text{F}(p,p\gamma_{1-0})^{19}\text{F}$	M.J. Kenny, Aust. J. Phys. 34 (1981) 35	Gurbich
20.06.13	$^9\text{Be}(p,p_2)^9\text{Be}$ $^9\text{Be}(p,p_0)^9\text{Be}$ $^9\text{Be}(p,\alpha_1)^6\text{Li}$ $^9\text{Be}(p,\alpha_0)^6\text{Li}$	H.R. Blieden+(1963), Jour. Nuclear Physics, Vol.49, p.209	EXFOR: F0167004 EXFOR: F0167003 EXFOR: F0167002 EXFOR: F0167002
20.06.13	$^{16}\text{O}(d,p\gamma_0)^{17}\text{O}$ $^{19}\text{F}(d,p\gamma_0)^{20}\text{F}$ $^6\text{Li}(d,p\gamma)^7\text{Li}$ $^{11}\text{B}(d,p\gamma)^{12}\text{B}$	G.A. Sziki+(2006), Jour. Nucl. Instrum. Methods in Physics Res., Sect.B, Vol.251, p.343	EXFOR: D4155005 EXFOR: D4155006 EXFOR: D4155002 EXFOR: D4155004
14.06.13	$^{\text{nat}}\text{Si}(p,p_0)^{\text{nat}}\text{Si}$	T.A. Belote+(1961), Jour. Physical Review Vol.122 (1961) p.920	A.Gurbich (sinpp0h.r33, sinpp0i.r33)
27.05.13	$^{13}\text{C}(p,p_0)^{13}\text{C}$	N.P. Barradas et al., Nucl. Instr. and Meth. B 316 (2013) 81	A.Gurbich (c3pp0k.r33, c3pp0l.r33)

Table 2. The references sent to NDS for digitizing and preparing R33 files.

No.	Reference	Paper title	Comment
1	G.Á. Sziki, A. Simon, Z. Szikszai, Zs. Kertész, E. Dobos, NIMB 251 (2006) 343	Gamma ray production cross sections of deuteron induced nuclear reactions for light element analysis	Table 3
2	H. van Bebber, L. Borucki, K. Farzin, Á.Z. Kiss, W.H. Schulte, NIMB 136-138 (1998) 72	Total cross section of the $^{14}\text{N}(d,p\gamma)^{15}\text{N}$ nuclear reaction for analytical applications	Fig. 4
3	A.K. Valter, I.I. Malakhov, P.V. Sorokin, A.I. Taranov, Izvest. Akad. Nauk S.S.S.R. Ser. Fiz. (in Russian) 22 (1958) 871.	Elastic scattering of protons by Si nuclei	Figs. 3-5
4	J.R. Leslie, I.G. Main, Nuovo Cimento 50B, 389(1967)	Proton capture by ^{23}Na yielding γ -rays from the giant resonance of ^{24}Mg	Fig.2 a,b
5	M.J.A.de Voigt, J. Grootenhuis, J.B. van Meurs, C. van der Leun, Nucl.Phys. A170, 449 (1971)	The reaction $^{23}\text{Na}(\alpha,\gamma)^{27}\text{Al}$: (I). Yield curve, excitation energies and branchings of ^{27}Al levels	Fig. 2
6	J.W. Maas, E. Somorjai, H.D. Graber, C.A. van den Wijngaart, C. van der Leun, P.M. Endt, Nucl.Phys. A301, 213 (1978)	Investigation of ^{28}Si Levels with the (α,γ) and (p,γ) Reactions	Fig. 3
7	P. H. Stelson, W.M. Preston Phys. Rev. 95, 974–981 (1954)	Resonant States of ^{24}Mg Excited by Protons on Sodium	Figs. 3,4
8	R.M. Freeman, G.S. Mani, Nuclear Physics Volume 51, February–March 1964, Pages 593–603	Levels in ^{23}Na from the alpha bombardment of ^{19}F	Figs. 2-7
9	N.P. Baumann, F.W. Proseaa, JR. W.G. Rean, R.W. Kaoz, Phys. Rev. 104 (1956) 376	Elastic Scattering of Protons from ^{23}Na	Fig. 2
10	H.R. Blieden, Nuclear Physics 49 (1963) 209	A study of the $^8\text{Be}(p,\alpha)^6\text{Li}$ reaction from 3.5 to 12.5 MeV	Figs.3,4
11	H.E. Gove, Nuclear Physics 49 (1963) 279	Proton capture gamma rays in the giant resonance region of Mg-24	Fig.2, Fig.3
12	B.D. Kern, L.W. Cocher, Phys. Rev. 104 (1956) 711	Gamma rays from the proton bombardment of phosphorus	Fig. 1
13	G. S. Mani, Nuclear Physics 60 (1964) 588	Study of the reaction $^7\text{Li}(p,\alpha_0)$ up to 12 MeV proton energy	Fig. 1
14	J.R. Leslie, I.G. Main, Nuovo Cimento 50B (1967) 389	Proton capture by ^{23}Na yielding γ -rays from the giant resonance of ^{24}Mg	Fig.2 a,b
15	P.B. Lyons, Nuclear Physics A130 (1969) 25	Total yield measurements in $^{24}\text{Mg}(\alpha,\gamma)^{28}\text{Si}$	Fig. 1
16	P.B. Lyons et al. Nuclear Physics A130 (1969) 1	Total yield measurements in $^{27}\text{Al}(p,\gamma)^{28}\text{Si}$	Fig. 6
17	H.B. Willard, J.K. Bair, J. D. Kington, T.M. Hahn, C.W. Snyder, F P. Green, Phys. Rev. 85 (1952) 849	The yield of gamma-rays and neutrons from the proton bombardment of fluorine	Fig. 1 (Fluorine gammas only)
18	T.W. Bonner, et al. Phys. Rev. 102 (1956) 1348	Neutrons and gamma rays from the alpha-particle bombardment of ^9Be , ^{10}B , ^{11}B , ^{13}C , and ^{18}O	Figs. 1,3 (only gammas)
19	S.E. Hunt, R.A. Pope, and W.W. Evans, Phys. Rev. 106 (1957) 1012	Investigation of the gamma radiation produced by	Figs 2,5,6

		irradiating ^{10}B with protons in the energy range 0.7 to 3.0 MeV	
20	K.J. Broström, T. Huus, and R. Tangen, Phys. Rev. 71 (1947) 661	Gamma-ray yield curve of aluminum bombarded with protons	Fig. 3
21	P. Dyer, Phys. Rev. C23 (1981) 1865	Cross sections relevant to gamma-ray astronomy: Proton induced reactions	Figs. 5-13
22	G. Demortier, J. Rad. Chem. 45 (1978) 459	Prompt gamma-ray yields from proton bombardment of transition elements (Ti to Zn).	Tabular data
23	I. Lombardo, L. Campajola, E. Rosato, G. Spadaccini, M. Vigilante, Nuclear Instruments and Methods in Physics Research B 302 (2013) 19–23	Measurement of differential cross sections in $\alpha+^9\text{Be}$ elastic scattering	Tabular data
24	M. Allab et al. Le Journal de Physique 31 (1970) 919	Etude des reactions $^{12}\text{C}(d,d)$, $^{12}\text{C}(d,p_0)$ et $^{12}\text{C}(d,p_1)$ á $1.4 < E < 2.3$ MeV	Fig. 4 lower row
25	M. Lambert, G. Dumazet, Ch. Benedetti, D. Gresillon, Acad. Sc. Paris 262 (1966).		Fig. 2
26	A.Z. El-Behay, M.A. Farouk, M.H. Nassef, I.I. Zaloubovsky, Il Nuovo Cimento XXXVIII No. 1 (1965) 52	Studies of (d, α) and (d,d) Reactions on ^{32}S	Fig. 2
26	H. Brändle, W.R. Wylie, F. Zamboni, W. Zych, Nucl.Phys. A151 (1970) 211	The isobaric analog pair $^{57}_{26}\text{Fe}$ - $^{57}_{27}\text{Co}$	Fig.1a
27	E. Arai, M. Futakuchi, H. Kamada, J. Komaki, T. Matsuzaki, M. Ogawa, Y. Oguri, Nucl.Phys. A378 (1982) 259	High-resolution measurements of analogue states in ^{57}Co	Fig. 1a, 1b
28	W.A.Watson, E.G.Bilpuch, and G.E.Mitchell , Phys.Rev. C24 (1981) 1992	High resolution measurement of proton resonances in ^{57}Co	Fig. 1,2,3
29	S.R. Kennett, L.W. Mitchell, M.R. Anderson, D.G. Sargood, Nucl. Phys. A363 (1981) 233	Cross-section measurements and thermonuclear reaction rates for $^{52}\text{Cr}(p,\gamma)^{53}\text{Mn}$ and $^{54}\text{Fe}(p,\gamma)^{55}\text{Co}$	

2.2. IBANDL/SigmaCalc development

The SigmaCalc web site was installed on the server of the University of Surrey (<http://www.surreyibc.ac.uk/sigmacalc/>)¹. The interface was renewed (Fig. 1) including the addition of a progress bar. The interface “About” section was tidied up and expanded. Furthermore, all the evaluations performed in the period 2011-2013 were added (see Table 3).

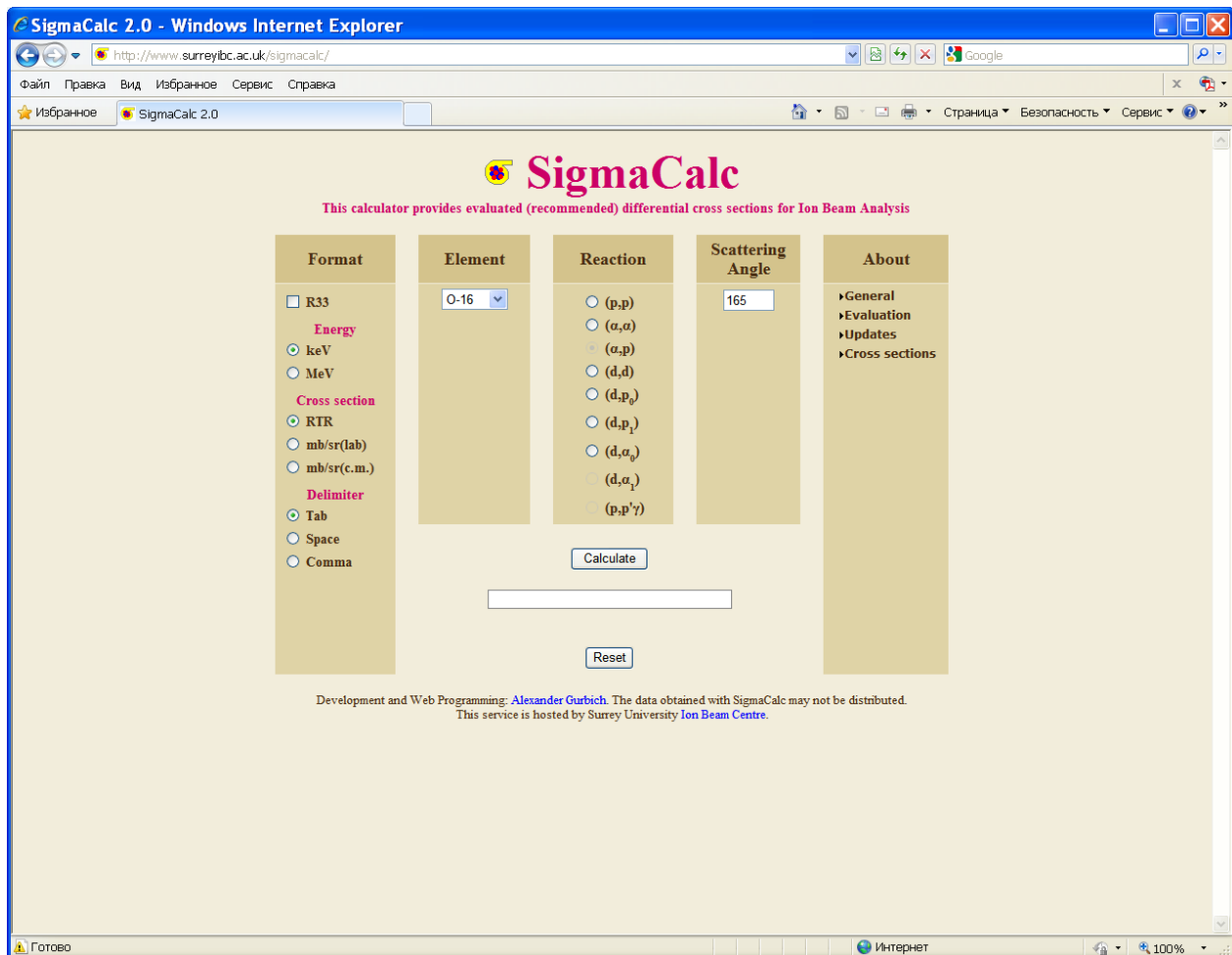


Fig.1. Interface of SigmaCalc

In order to provide users with the possibility to compare evaluated differential cross sections with the available results of experiments on the new SigmaCalc web page, the calculated cross sections are presented in a table (Fig. 2) which also contains experimental data taken from the current version of the IAEA IBANDL web site (<http://www-nds.iaea.org/ibandl/>) through a direct call to the IAEA web server. In the case of PIGE data, this feature also gives the possibility to compare evaluated data both with experimental cross sections and with thick target yields, the evaluated cross sections being converted into the thick target yield on the fly (Fig. 3).

The IAEA IBANDL interface, on the other hand, now offers two options for obtaining evaluated cross-section data: a) pre-calculated evaluated cross-section data using the SigmaCalc versions 1.6 and 2.0 provided to the IAEA by A. Gurbich until October 2013, and b) ‘on-the-fly’ calculations using the

¹ Due to new stringent IT security measures, the IAEA NDS Web server is no longer accessible for editing by external users hence the decision to install SigmaCalc on another Web server.

version of SigmaCalc available on the University of Surrey web server through direct calls to this server.

Table 3. SigmaCalc updates as displayed on the SigmaCalc web page.

Date	What's new in SigmaCalc
01.09.2013	The evaluated cross section for $^{23}\text{Na}(p,p)^{23}\text{Na}$ was added
05.06.2013	$^1\text{H}(a,p)$ - extended up to 12 MeV $^4\text{He}(p,p)$ - extended up to 3.0 MeV, energy step decreased $^{12}\text{C}(a,a)$ - revised (NIMB 296 (2013) 87) $^{12}\text{C}(d,p0)$ - revised (NIMB 301 (2013) 41) $^{13}\text{C}(p,p)$ - new evaluation (to be published in NIMB) $^{16}\text{O}(d,p0)$ - revised $^{16}\text{O}(d,p1)$ - revised $\text{natMg}(a,a)$ - added $^{28}\text{Si}(a,a)$ - revised (presented at Nuclear Data Conference in New York, 2013) $\text{natSi}(a,a)$ - revised (presented at Nuclear Data Conference in New York, 2013) $^{28}\text{Si}(p,p)$ - revised, energy range extended up to 3.5 MeV $\text{natSi}(p,p)$ - revised, energy range extended up to 3.5 MeV $\text{natFe}(p,p)$ - added
05.06.2013	An updated 2.0 version has been established at the Surrey University Ion Beam Centre server.

$^{16}\text{O}(\alpha, \alpha_0)^{16}\text{O}$

Home

The experimental data presented in the table is an excerpt from [IBANDL](http://www-nds.iaea.org/ibandl/) database maintained by the IAEA.

No.	Angle	Energy(keV)	Reference	File	Plot
1	170	2020-3980	Evaluated cross-section <input type="button" value="Calculate"/>	<input type="button" value="File"/>	<input type="checkbox"/>
2	175.7°	5000-12390	J.John+(1969), Jour. Physical Review, Vol.181, p.1455	<input type="button" value="File"/>	<input type="checkbox"/>
3	175.0°	8300-8900	Cheng Huan-Sheng et al. Acta Physica Sinica v.2 (1993) 641	<input type="button" value="File"/>	<input type="checkbox"/>
4	170.00°	1770-5030	Leavitt, J.A., McIntyre Jr., L.C., Ashbaugh, M.D., Oder, J.G., Lin, Z. and Dezfouly-Arjomandy, B. Nucl. Instr. and Meth. B44 (1990) 260.	<input type="button" value="File"/>	<input type="checkbox"/>
5	170.00°	1810-2920	J.A.Leavitt and P.Stoss, Nucl. Instrum. Methods B15 (1986) 296	<input type="button" value="File"/>	<input type="checkbox"/>
6	170.00°	2000-9000	Cheng, H.-S., Shen, H., Tang, J. and Yang, F. Nucl. Instr. and Meth. B83 (1993) 449	<input type="button" value="File"/>	<input type="checkbox"/>
7	170.0°	2000-9000	Cheng Huan-Sheng et al. Acta Physica Sinica v.2 (1993) 641	<input type="button" value="File"/>	<input type="checkbox"/>
8	170.00°	2430-6010	J. Demarche and G. Terwagne, J. Appl. Phys. 100, 124909 (2006)	<input type="button" value="File"/>	<input type="checkbox"/>
9	170.00°	2810-3960	J.A.Leavitt and P.Stoss, Nucl. Instrum. Methods B15 (1986) 296	<input type="button" value="File"/>	<input type="checkbox"/>
10	170.00°	3450-4950	J.A.Leavitt and P.Stoss, Nucl. Instrum. Methods B15 (1986) 296	<input type="button" value="File"/>	<input type="checkbox"/>
11	170.00°	7300-7650	J.A.Davies, F.J.D.Almeida, H.K.Haugen, R.Siegele, J.S.Foster, T.E.Jackman Nucl. Instrum. Methods B85 (1994) 28	<input type="button" value="File"/>	<input type="checkbox"/>
12	170.0°	8300-8900	Cheng Huan-Sheng et al. Acta Physica Sinica v.2 (1993) 641	<input type="button" value="File"/>	<input type="checkbox"/>
13	170.00°	12640-13440	Caskey et al. Phys. Rev. C31 (1985) 717	<input type="button" value="File"/>	<input type="checkbox"/>
14	169°	6020-7970	H.Yonezawa+(1994), Jour. Nucl. Instrum. Methods in Physics Res., Sect.B, Vol.88, p.207	<input type="button" value="File"/>	<input type="checkbox"/>
15	167°	5210-5980	C.J.Wetteland et al. LA-UR-98-4867	<input type="button" value="File"/>	<input type="checkbox"/>
16	166°	3320-3400	E.Berthoumieux+(1998), Jour. Nucl. Instrum. Methods in Physics Res., Sect.B, Vol.136-138, p.55	<input type="button" value="File"/>	<input type="checkbox"/>
17	165.70°	5030-12450	John, J., Aldridge, J.P. and Davis, R.H. Phys. Rev. 181 (1969) 1455	<input type="button" value="File"/>	<input type="checkbox"/>
18	165.2°	3730-6480	L.C.Mcdermott+(1960), Jour. Physical Review, Vol.118, p.175	<input type="button" value="File"/>	<input type="checkbox"/>
19	165.00°	2010-2790	R.A.Jarjis, Nucl. Instrum. Methods B12 (1985) 332	<input type="button" value="File"/>	<input type="checkbox"/>
20	165.00°	2050-9010	Feng et al., 1994 (see Comment)	<input type="button" value="File"/>	<input type="checkbox"/>
21	165.00°	2430-6010	J. Demarche and G. Terwagne, J. Appl. Phys. 100, 124909 (2006)	<input type="button" value="File"/>	<input type="checkbox"/>
22	165.00°	2800-3570	R.A.Jarjis, Nucl. Instrum. Methods B12 (1985) 332	<input type="button" value="File"/>	<input type="checkbox"/>

Fig. 2. Presentation of the evaluated cross sections along with an excerpt from IBANDL data library (<http://www-nds.iaea.org/ibandl/>).

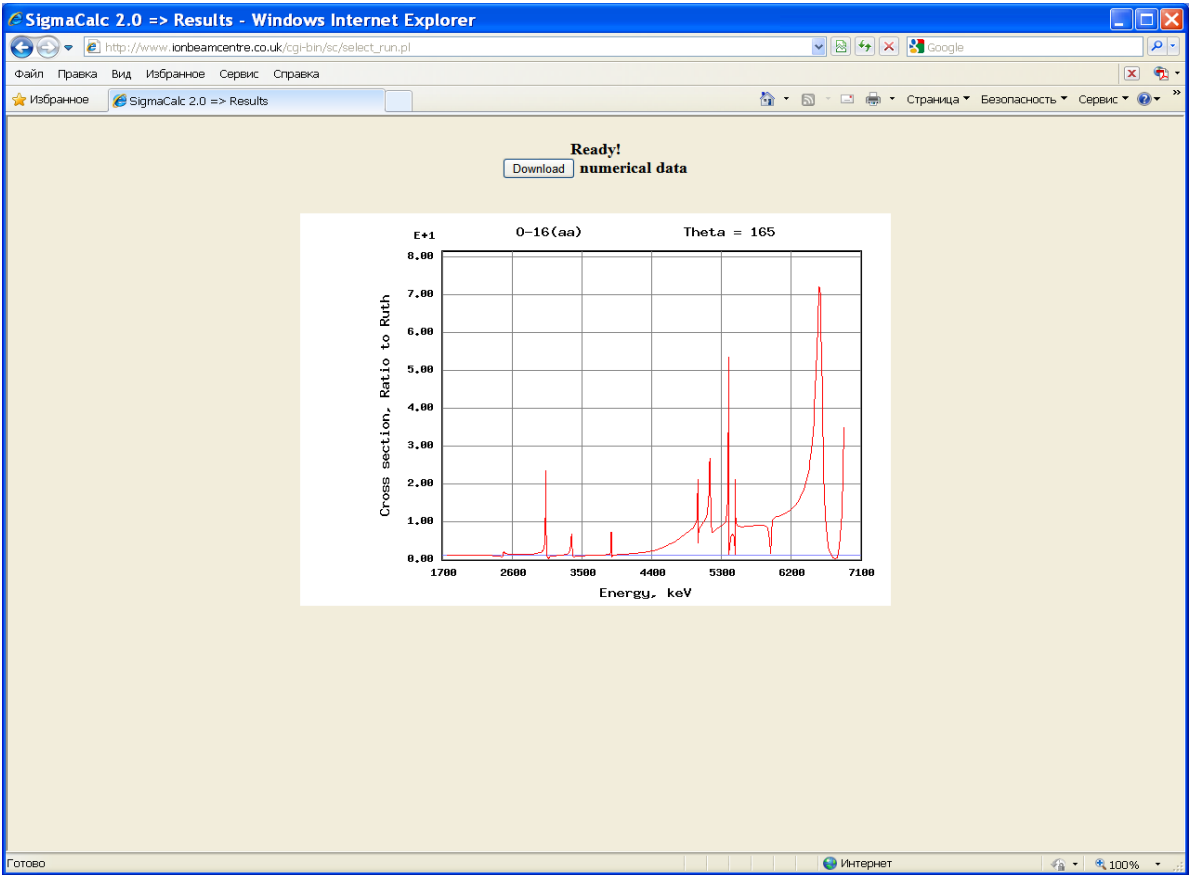


Fig. 3. Presentation of the results of SigmaCalc calculations.

2.3. Evaluation of charged particle reaction cross sections

2.3.1. The $^{12}\text{C}(d,p_0)^{13}\text{C}$ cross section

Carbon depth profiling presents a strong analytical challenge for all the major Ion Beam Analysis (IBA) techniques, with NRA (Nuclear Reaction Analysis) being widely implemented, via the use of the $^{12}\text{C}(d,p_0)^{13}\text{C}$ reaction. As a consequence, there exist several experimental differential cross-section datasets in the literature for energies and angles suitable for NRA. In the present work the evaluation for this reaction was made for deuteron beam energies between 0.8 and 2 MeV, in the framework of DWBA (Distorted Wave Born Approximation) and R-matrix calculations. The contributions of the direct and compound reaction mechanisms are analyzed, and the evaluated results are benchmarked using a thick, mirror-polished, glassy carbon target at different deuteron beam energies and detector angles.

In the present work, the code DWUCK4, developed by P. Kunz [3] has been adopted for the DWBA calculations. The code calculates the scattering and reaction observables for binary nuclear reactions following a zero-range interaction. In its initial form, it provides as output the angular distribution of the cross section for a specific bombarding energy. The parameters adopted for the calculations generally follow the systematic described in [4], despite the fact that the energy range (0.4-0.85 MeV) is rather low, and does not fully correspond to the energy range which is covered in the present evaluation. On the other hand, the systematic developed by Satchler in [5] refers to higher deuteron beam energies (3-8 MeV), where the direct reaction mechanism has a more profound contribution. As a result, intermediate values were finally adopted for the optimal potential parameters which are listed in Table 5. These values are comparable with those reported in the past by [6] and [7]. A typical angular distribution for $E_{d,\text{lab}}=1000, 1500$ and 2000 keV is presented in Fig. 6, where all the angles are given in the cm system. The existence of strong variations is evident, but it is also worth to note the increase of the cross section with increasing beam energy for the very steep backward detection angles ($\theta > 150^\circ$), which are of particular interest for NRA applications.

Table 5. Optimal potential parameters for the incoming and outgoing charged particle channels, used in the DWUCK4 code for the DWBA calculations. The columns correspond to the strength of the real potential, its reduced radius, its diffuseness, the spin-orbit factor and the strength of the imaginary potential in the derivative Woods-Saxon form case, following the usual notation.

Potential	V (MeV)	r_0 (fm)	α (fm)	V_{so} factor	W (derivative W-S, MeV)
d	130.15	0.9	0.9	0.0	2.325
p	51.69	1.3	0.34	10.53	0.0

In order to facilitate the evaluation process, DWUCK4 was included as an additional subroutine in the main code performing R-matrix calculations. As a consequence, the results were accordingly modified as to provide excitation functions for a specific angle, and thus the contribution of the direct mechanism could be compared over the whole energy range covered by the present work for a specific detection angle, as shown in Fig. 7 for 170° . Although the complicated resonant structure clearly prevails, it is also evident that there is an ever increasing trend of the direct component with energy, despite the existing fluctuations.

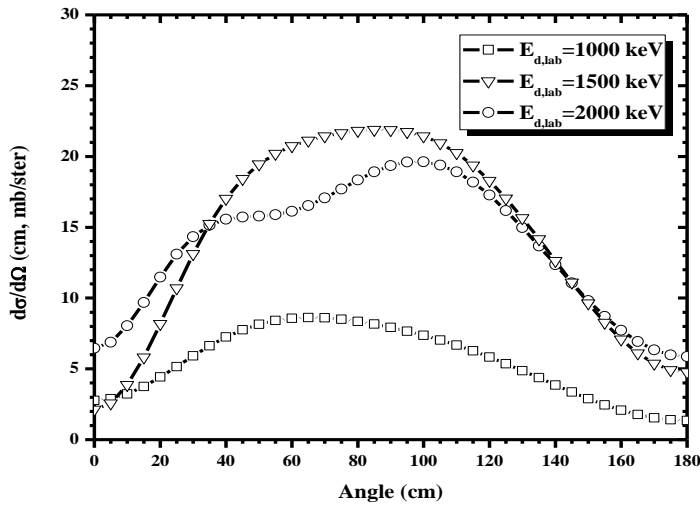


Fig.6. Angular distributions of the direct mechanism contribution (in the cm system) following DWBA calculations using the code DWUCK4 for $E_{d,lab}=1000, 1500$ and 2000 keV.

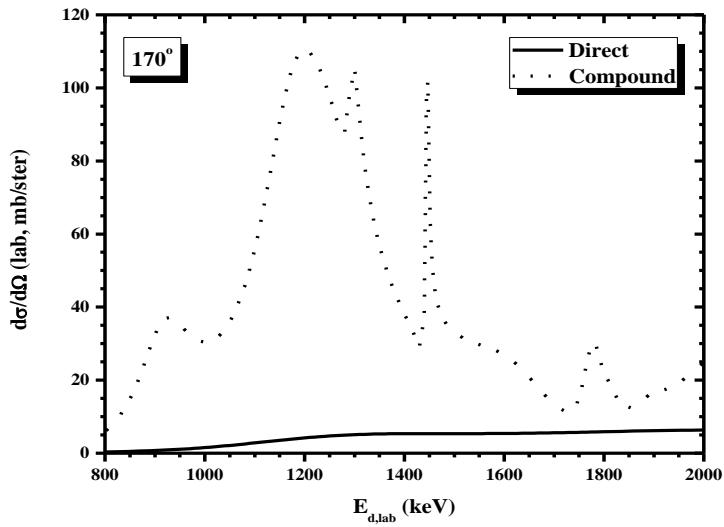


Fig. 7. Demonstration of the direct versus compound mechanism contribution for the scattering angle of 170° , over the whole energy range covered in the present evaluation.

The R-matrix theory [8] is generally accepted as the most appropriate one for the analysis of resonance reactions in low-energy nuclear physics. In this approach, the configuration space of the scattering problem is divided into an internal region, corresponding to the compound nucleus, where the total wave function can be expanded into a complete set of eigenstates (in terms of unknown base functions, with the energy eigenvalues and the matrix elements of the base functions being adjustable parameters) and an external region, where the possible combinations of coupled particle pairs exist, corresponding to the reaction channels that emerge from the compound nucleus. This division of space is made by the choice of the boundary of the compound nucleus, i.e. an appropriate nuclear radius is chosen for each reaction channel. The wave functions of the internal and external regions, and their derivatives, must match at the boundary surface. The R-matrix takes account of all the interactions which occur inside the nucleus. The external region is generally assumed to contain only long-range interactions between the particles, and thus, has a complete analytical solution. The hard-sphere scattering phase shifts are conventionally used for the external wave functions, and they were adopted in the present work as well. In the particular case of ^{12}C , the calculations are relatively simplified by the fact that it is an even-even nucleus ($J^\pi=0^+$).

The evaluation starts with an assessment of the available data. This data assessment is critical, especially in the cases where large discrepancies exist. Nevertheless, in the case of the $^{12}\text{C}(d,p_0)^{13}\text{C}$ reaction, despite the existence of a vast number of experimental cross section datasets, the deviations between different points for the same beam energy and detection angle do not exceed 30%, with the only critical exception existing at energies near or above $E_{d,\text{lab}}=2$ MeV. More specifically, differential cross-section datasets and angular distributions from [9] and [10-24] were mainly considered for the evaluation. In the case of [15], the differential cross-section data, as taken from IBANDL, had to be divided by a constant factor equal to 1.85, in order to be in accordance with the main bulk of the other available experimental datasets.

The positions of the corresponding resonances, as well as the widths, Γ , and the J^π assignments that are used as input in the code, were taken from nuclear reviews and compilations, such as [25] and [26], with certain modifications, while the partial widths Γ_p , and the spin mixing parameters were tuned inside the code in order to be in accordance with the main bulk of experimental data. Two notable exceptions concerned: (a) The addition in the calculations of a relatively broad, low-energy resonance ($E_{d,\text{lab}}\sim 809$ keV, $\Gamma=192$ keV) which has not been observed in the past in the $d+^{12}\text{C}$ system, but rather in the $p+^{13}\text{C}$ one, yielding the same compound nucleus [26], and (b) The large increase in the width Γ of the broad, high-energy resonance ($E_{d,\text{lab}}\sim 2.205$ MeV, $\Gamma\sim 500$ keV), which could be partly justified by the existence of another overlapping broad resonance observed in the past in [14] around 2.05 MeV, which is present in literature concerning the $^{12}\text{C}(d,n)$ reaction, but is not mentioned, or included in [25, 26]. With these two modifications the evaluation succeeded in reproducing the high-end and the low-energy tail of the benchmarking spectra, as analyzed in the following section. The results for the resonance parameters are summarized in Table 6.

Table 6. Resonance parameters used as input for the R-matrix calculations.

E_R (lab, MeV)	Γ (keV)	Γ_p/Γ	J^π	ϵ
0.809	192	0.005	1^-	1
0.915	150	0.428	1^+	0
1.150	200	0.600	1^-	1
1.200	264	0.517	2^-	1/3
1.295	30	0.304	1^+	0/2
1.450	7	0.167	3^+	2
1.670	180	0.059	2^-	1
1.815	120	0.111	2^-	1
1.910	101	0.841	1^-	1
2.205	500	0.860	2^-	1

A detailed comparison of the evaluated results with selected available experimental datasets for the detection angles of 165° is presented in Fig. 8. More results for different angles can be found in SigmaCalc. In most of the cases the evaluation tends to produce relatively lower values than most experimental datasets, in order to remain in accordance with the benchmarking results, especially in the high-energy part (while for low deuteron beam energies, and especially in the ‘plateau’ between $E_{d,lab} \sim 800-1050$ keV the evaluation closely follows the bulk of experimental data). Thus, in effect, the evaluation process could be described as re-iterative, as far as the compound nucleus mechanism contribution was concerned. This contribution to the reaction cross section was incoherently added to the direct one (determined as described in the previous section), and was subsequently compared to the experimental cross-section datasets and tested against the benchmarking spectra for the fine-tuning of the code’s input parameters.

As it has already been shown in the past, it is practically imperative to test the reliability of the obtained evaluated results, through a rigorous benchmarking process. Moreover, the results of the benchmarking experiments can also provide the necessary feedback for the fine tuning of the optimal model parameters and this justifies the claim that the theoretical evaluation is indeed a dynamical process.

The experiments were performed using the deuteron beam of the 5.5 MV TN11 Tandem Accelerator of N.C.S.R. “Demokritos”, Athens, Greece. Experimental details can be found elsewhere [27]. The final benchmarking results are shown in Figs. 9, and 10 for 155° and 170° respectively, where only the high-energy part of each spectrum, corresponding to the emitted protons, is shown. The solid line represents the simulations using the evaluated differential cross-section datasets, while the experimental points are denoted by open circles. The agreement between the experimental spectra and the evaluated results is quite satisfactory for both detection angles and over the whole energy range studied in the present work. More specifically, the experimental spectra are reproduced with accuracy better than $\sim 5-7\%$ (comparing the total integrated experimental and evaluated yield). The

point-by-point agreement is also satisfactory, taking into account the experimental errors, as well as, the possible uncertainties in the stopping power values and in the determination of the correct mathematical behavior of the adopted beam energy straggling model.

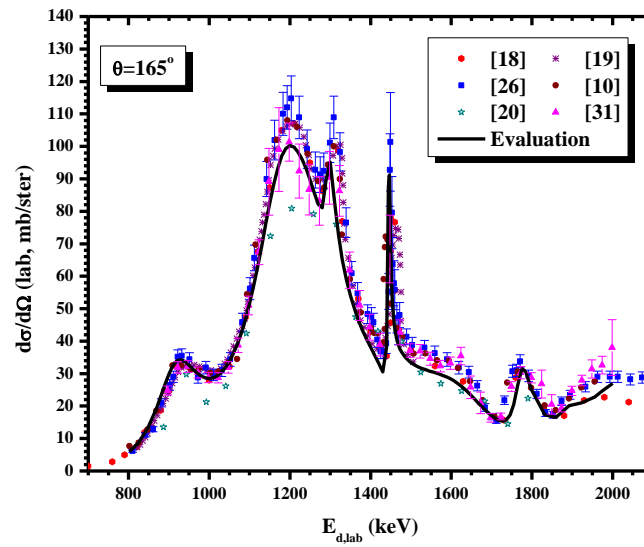


Fig. 8. Experimental cross section datasets, along with the corresponding evaluated values, at 165° .

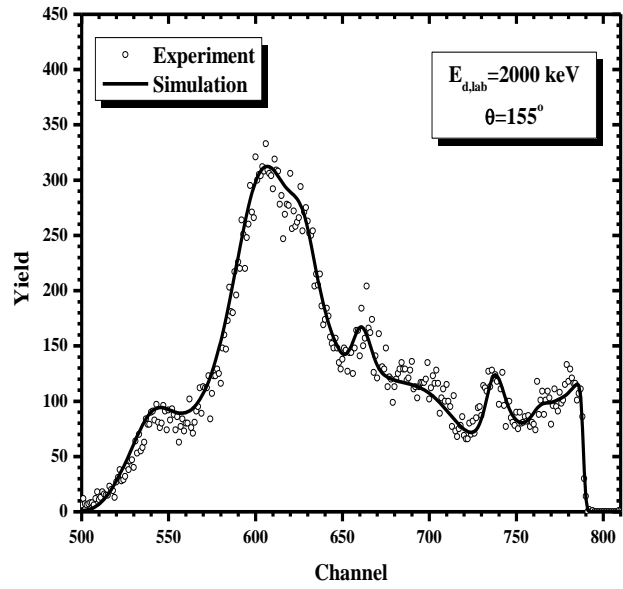
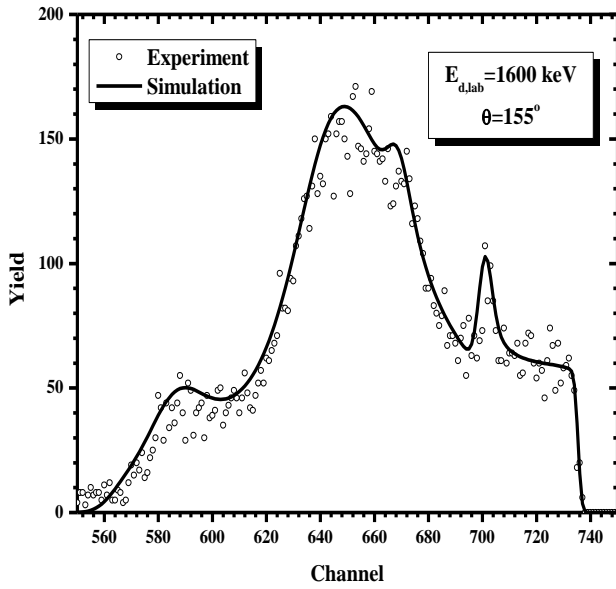


Fig. 9. Benchmarking results for $E_{d,lab}=1600$ keV (left) and 2000 keV (right), with the detector set at 155° .

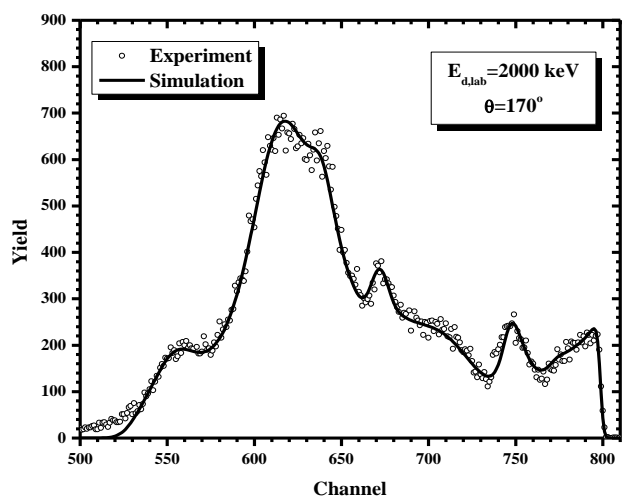
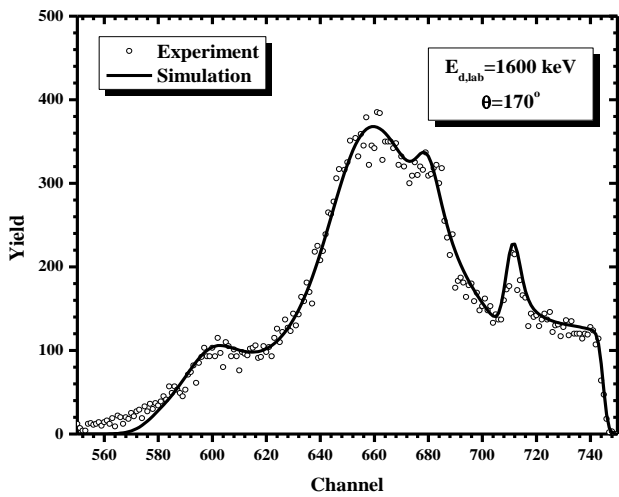


Fig. 10. Benchmarking results for $E_{d,lab}=1600$ keV (left) and 2000 keV (right), with the detector set at 170° .

2.3.2. The $^{28}\text{Si}(\alpha,\alpha_0)^{28}\text{Si}$ and $^{\text{nat}}\text{Si}(\alpha,\alpha_0)^{\text{nat}}\text{Si}$ cross sections

The differential alpha elastic scattering cross sections for silicon at low energy were found in six papers [28-33]. The excitation functions were obtained in the energy range from 3.6 to 5.8 MeV for 19 different angles from 173° down to 82° in [28], at angles from 130° to 170° with 10° step in the energy interval of 3.1 to 7.7 MeV in [29], and at four angles (168° , 126° , 89° , 70°) in the energy region of 4.9-11.7 MeV in [30]. For the work [31] the data are available only for 165° in the energy range from 2.5 to 6.0 MeV. Also in [32-33] the data were measured for only one angle (170° in [32] and 172° in [33]) in the energy range of 2.0-9.0 and 3.8-4.6 MeV respectively. Natural silicon (92.23% of ^{28}Si , 4.67% of ^{29}Si , and 3.10% of ^{30}Si) was used for manufacturing targets in all the cases. The accuracy of the measured data was reported to be $\sim 3\text{-}7\%$.

The measurements carried out in all the works but one ([28]) were performed with thin targets. In [28] the cross section was derived from the spectra of alphas elastically scattered from a thick target. It should be noted that the energy step in thin target measurements significantly exceeded a typical width of the resonances specific for the case studied and the resonance structure was smeared due to energy straggling in the thick target measurements. The work [28] is the only one where the resonance parameters for $\alpha+^{28}\text{Si}$ were derived from the experimental data. These parameters are listed in the compilation [34]. A striking discrepancy between corresponding energy level parameters of ^{32}S is observed in the comparison of [34] with the compilation [35].

The R-matrix theory was employed in order to calculate the $^{28}\text{Si}(\alpha,\alpha)^{28}\text{Si}$ cross sections. In the calculations the phases obtained in the frameworks of the optical model with Saxon-Woods real potential well and a surface absorption were taken instead of hard sphere ones in order to take into account tails of broad single particle resonances. Explicit formulas can be found elsewhere [8]. Cross section for natural silicon was calculated as a weighted sum of the cross sections of its three stable isotopes according to their abundance. As far as minor silicon isotopes produce only small contribution to the sum the cross sections for them were assumed to be Rutherfordian.

The spectra of backscattered alphas were calculated with account of all the broadening effects. For a given projectile energy the corresponding depth x where the energy of the slowing down particle reaches energy E was calculated for each of the $d\sigma(E)/d\Omega$ values, stopping power for alphas in silicon being taken from [42]. Then a convolution of $d\sigma(E)/d\Omega$ with a function representing energy spreading was made. Bohr's theory was assumed for energy straggling. Another convolution was applied in order to take into account energy spreading for the outgoing particle and the detector resolution.

The measurements were done using a 2 MV Tandetron of Surrey University Ion Beam Centre. Two surface barrier detectors were located at scattering angles of $149:2^\circ$ and $172:8^\circ$ determined using a beam line laser. The solid angles subtended by the detectors were 3.50 and 1.25 msr respectively. Electronics calibration was made with an Au/Ni/SiO₂/Si sample as described in [43]. Beam current was 40 nA with a nominal size of the beam spot on the target of 1 mm. An amorphised Si sample was used, the amorphisation being achieved with a multiple energy ^{28}Si implantation up to 2 MeV on a LN₂ cooled stage. The sharp $^{12}\text{C}(\alpha,\alpha)^{12}\text{C}$ resonance at 4262 keV and $^{16}\text{O}(\alpha,\alpha)^{16}\text{O}$ resonance at 3038 keV were used to verify the machine energy calibration. The absolute beam energy uncertainty was estimated to be about 4 keV. Totally 97 spectra were measured in the energy interval of 3.7-6.1 MeV.

The comparison of the evaluated cross section with the available experimental data in the vicinity of 170° is presented in Fig. 11 whereas the comparison of the measured and simulated spectra is shown in Fig. 12. As is seen from the figures the theoretical results are in a good agreement with experiment. The resonance parameters used in the calculations are listed in Table 7. These parameters significantly differ from [36]. An attempt to reproduce the cross sections and spectra using parameters obtained in [36] gave unsatisfactory results in both cases. It is strange enough that

the elastic alpha width in [36] constitutes only small fraction of the total width for the majority of the resonances. Except for (α,γ) with normally very small width the only competitive channel is $^{28}\text{Si}(\alpha,p)^{31}\text{P}$ ($Q = -1.916$ MeV), however calculations with parameters from [36] produce unrealistically large cross section for this channel and the corresponding protons are not observed in the measured spectra.

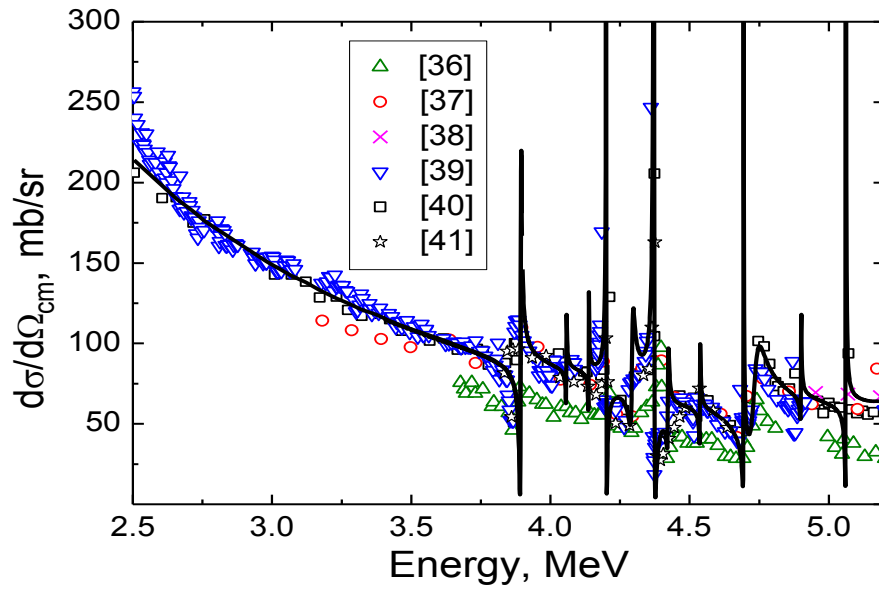


Fig. 11. The evaluated cross sections and the available experimental data for alpha elastic scattering from silicon at $\sim 170^\circ$.

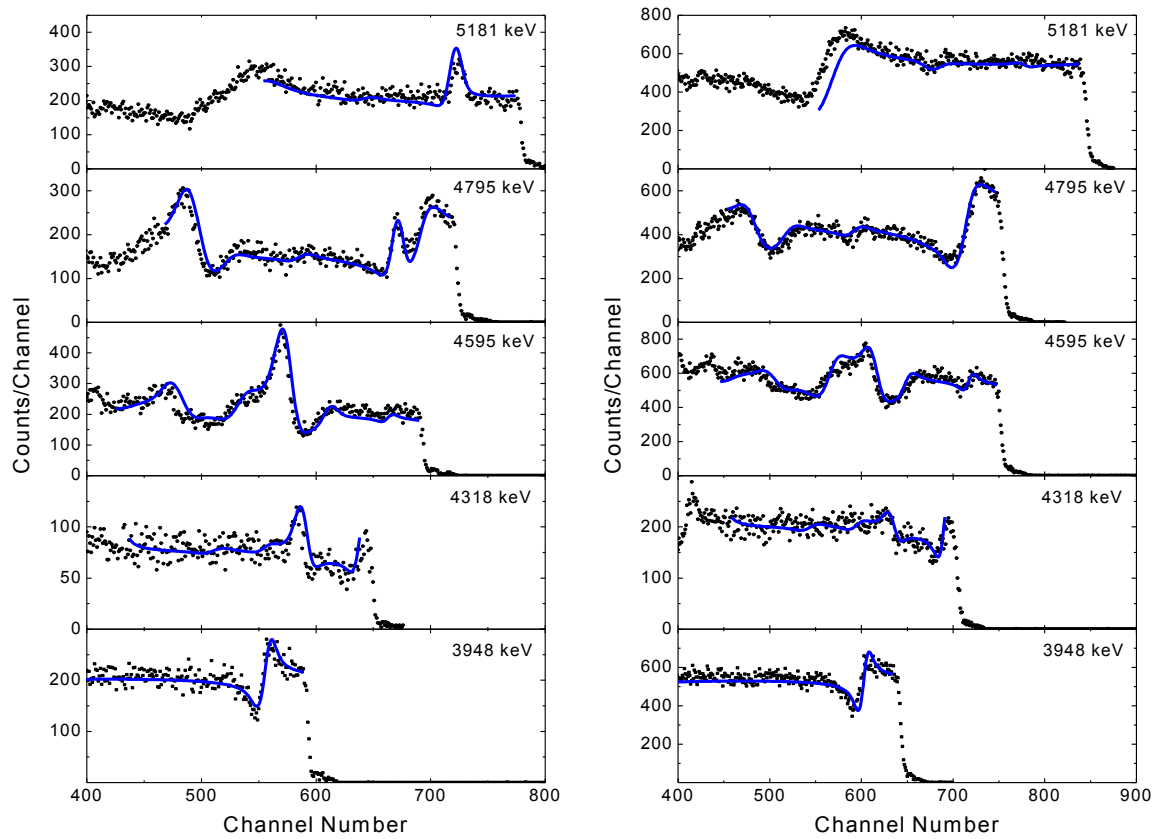


Fig. 12. Comparison of measured and calculated spectra for scattering angles of 172:8° (left) and 149:2° (right).

Table 7. The optimal resonance parameters for $^{28}\text{Si}(\alpha,\alpha)^{28}\text{Si}$.

E_{lab} , keV	3876	4059	4139	4200	4309	4381	4430	4540	4693	4821	4900	5069
J^π	1^-	0^+	0^+	3^-	0^+	3^-	0^+	0^+	5^-	0^+	2^+	5^-
Γ_{lab} , keV	3.6	1.7	1.2	1.3	8.9	3.3	4.7	1.9	0.6	67.0	2.1	0.6

2.3.3. The $^{13}\text{C}(p,p_0)^{13}\text{C}$ cross section

In the data found in the literature, one single experiment by Latorre et al., at 125° , covers a wide energy range, from 1.00 to 2.58 MeV [44]. Milne covered the range 0.45-1.62 MeV at 158.4° [45]. Gerke et al. measured three energy points only, 1.55, 1.92, and 2.38 MeV [46]. Zipoy et al. measured the cross section from 1.63 to 3.31 MeV at 146.5° [47]. Finally, Kim et al. measured at 85.6° an angle not usual in EBS, in the energy range from 1.58 to 4.38 MeV [48], and Kashy et al. measured at higher energies, from 2.61 to 4.99 MeV, at a 163.8° angle [49].

However, the existing scattering cross section data are unsatisfactory. Not because all the data date from the 1950s and 1960s, but because there is a strong dispersion of data, and it is unclear whether this is due to the angular dependence of the cross section. In some energy ranges that do not have strong sharp resonances the data dispersion is more than a factor of 2. On the other hand, at the resonances, comparing for instance the data of Latorre et al. with the data of Zipoy et al. at 125° and 146.5° , respectively, we see that at the 2.11 MeV resonance the 125° data is lower than the 146.5° data, but at the 1.98 MeV resonance this is the other way around, with the 125° cross section 40% higher than that collected at 146.5° . On the other hand, the data collected at 85.6° does not show evidence of resonances at those energies, but it presents a strong minimum at 2.38 MeV, which is absent in all the other data sets.

In order to overcome the above-mentioned problems, a new measurement was performed with the aim to determine the elastic scattering cross section of protons in ^{13}C at 140° and 160° scattering angles in the energy range 0.8 to 2.43 MeV, using a ^{13}C thin film on a natural carbon substrate [50]. The scattering cross sections determined for 140° and 160° scattering angles are shown in Fig. 13. A strong angular dependence of the cross section at the resonances is observed. At the 1.462 resonance, the 160° results are close to those determined by Milne [45] for 158.4° . However, at the 1.98 and 2.11 MeV resonances, both the 140° and 160° results are higher than the values reported by Zipoy et al. [47] for the intermediate angle 146.5° .

The calculations of the cross section were made in the framework of the R-matrix theory combined with the optical model. The optimisation of the free parameters of the model was made taking account of the data [50] along with all the information found in the literature. The optimal parameters are listed in Table 8. The evaluated cross section is compared with the experimental data in Fig. 13. Complementary measurements were made using a different experimental setup that also has one detector located at a 140° scattering angle. The proton beam energy was varied in small steps around the 1.462 MeV resonance. Some of the data collected are shown in Fig. 14, together with simulations produced using the evaluated ^{13}C cross section determined in this work. The determined sample thickness and composition were used, together with cross sections for ^{12}C , N and O from SigmaCalc. That is, the simulations shown are not fits to the data, and the excellent agreement constitutes a benchmark that confirms the validity of the evaluated cross sections.

Table 8. The optimal resonance parameters for $^{13}\text{C}(p,p)^{13}\text{C}$.

E_{lab} , keV	551	1152	1420	1462	1523	1540	1990	2110	2337	2743	2885	3105
J^π	1^-	0^+	0^-	3^-	5^+	2^+	3^-	2^-	1^-	1^+	2^+	2^+
Γ_{lab} , keV	40	4.2	690	20	1.0	9.0	4.7	55	15	12.0	80	33

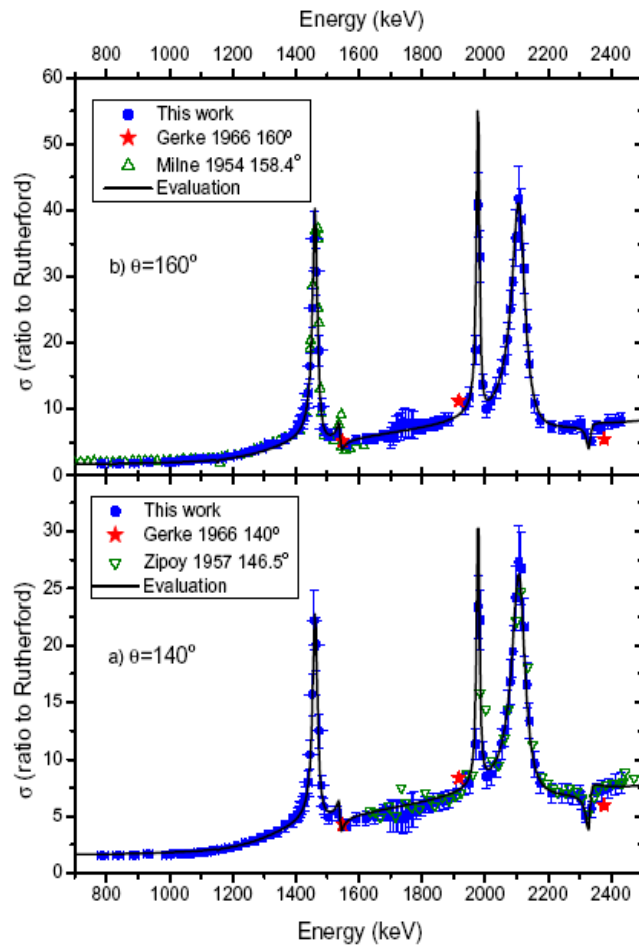


Fig. 13. The $^{13}\text{C}(p,p)^{13}\text{C}$ cross sections at (a) 140° and (b) 160° . Blue dots present data [50], red stars are data from [46], and green triangles are data [47].

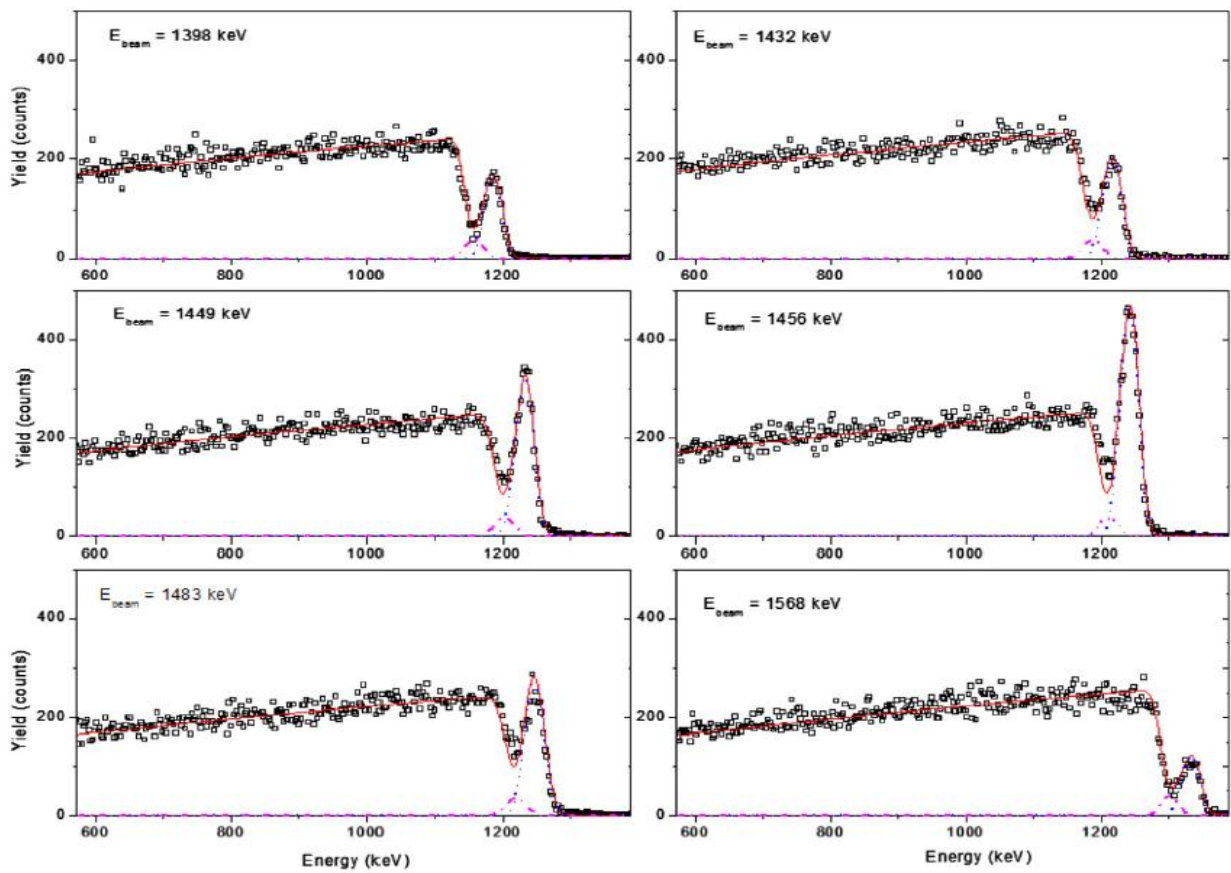


Fig. 14. Six out of 17 spectra collected to benchmark the cross section determined in this work for 140° scattering angle, around the 1.462 MeV resonance. Solid lines are simulations using the evaluated $^{13}\text{C}(p,p)^{13}\text{C}$ cross section. Dashed lines are the simulated ^{13}C signal. Dash-dotted lines are the simulated signal from the ^{12}C within the ^{13}C film.

2.4. Evaluation for PIGE

The feasibility of the extension of the evaluation over PIGE data was investigated. Two different cases were studied – gamma emission accompanying inelastic scattering of protons ($p,p'\gamma$), and proton radiative capture, i.e. (p,γ)-reaction.

The ($p,p'\gamma$) reaction is possible only if the projectile energy exceeds the first energy level in the target nucleus. This type of reaction is actually inelastic scattering accompanied by γ -emission from the residual nucleus. In a (p,γ) reaction, γ rays of different energies are emitted corresponding to transitions to different levels of the residual nucleus. Because, in addition to its kinetic energy, the proton brings to the compound nucleus its binding energy (which is, on average, ~ 8 MeV), the compound nucleus becomes highly excited. The excitation energy E_x is

$$E_x = \frac{M_2}{M_1 + M_2} E_0 + Q,$$

where E_0 is the initial proton energy; Q is the reaction energy; and M_1 and M_2 are the projectile and target nucleus masses, respectively. The energy for the emitted primary γ rays is calculated as

$$E_\gamma^{(i)} = E_x - E_{\text{level}}^{(i)},$$

where E_{level} is the energy of the excited state in the residual nucleus. In addition to the primary gamma quanta, a cascade of γ rays corresponding to the transitions between the levels of the residual nucleus is also emitted. Their energies are calculated as the differences between the respective level energies. The branching ratios and other detailed information on levels and gammas can be found in the literature and in the electronic databases. It should be noted that the data presented in various sources might be slightly different because each of the data files is obtained as a result of the analysis of many sets of experimental data that are not necessarily consistent; moreover, the derived parameters depend on the approach employed.

2.4.1. The $^{23}\text{Na}(p,p_1\gamma)^{23}\text{Na}$ cross section

The intense 440 keV gamma-ray emission of the $^{23}\text{Na}(p,p_1\gamma)^{23}\text{Na}$ reaction is very convenient for PIGE and so it is often used in analytical work. However, only few papers were found where information on the corresponding cross section or yield suitable for evaluation was published [51-55]. The measurements in [51] were performed in the energy range from 1.25 to 2.40 MeV. The target used in the work consisted of a thin film of NaCl ($14.4 \mu\text{g}/\text{cm}^2$) evaporated on a self-supported thin film of Ag. The normalization of the cross section was made against Rutherford backscattering from Ag, the Na/Ag number of atoms ratio being defined by RBS with alpha particles. The γ -radiation was detected by an HPGe detector, located at an angle of 120° to the beam axis. The absolute efficiency was determined by means of calibrated radioactive sources placed at the target position. It is important that the beam energy loss in the target was less than a typical width of the resonances in the reaction under investigation and the cross section was measured with sufficiently small energy steps. The results of the measurements were presented as total cross sections calculated assuming an isotropic angular distribution of the 440 keV gamma-ray emission. The authors assigned an uncertainty of 7% to the results.

In [52] the differential cross section for γ -ray emission from the reaction $^{23}\text{Na}(p,p_1\gamma)^{23}\text{Na}$ was measured at 135° for proton energies from 2.2 to 5.2 MeV with steps ranging from 20 to 5 keV using a $63 \mu\text{g}/\text{cm}^2$ NaBr target evaporated on a self-supporting thin C film. The proton energy loss in the NaBr film ranged from about 5 to 3 keV. The methodology of normalization was similar to [51]. The overall uncertainty for absolute cross section was estimated to be $\pm 12\%$.

The yield of 440 keV gammas from a thick NaCl target was measured in [53] at 90° in the energy range of 0.8 – 2.7 MeV. The data were reported as the number of gamma quanta per $1 \mu\text{C}$ emitted into a unit solid angle.

The excitation curve for the gamma emission from the $^{23}\text{Na}(p,p_1\gamma)^{23}\text{Na}$ reaction was measured in [54] in the energy range from 0.98 to 2.08 MeV at 55° . The target was thin and the target material was Na_2WO_4 . The results were presented as a plot in non-normalized units. Unfortunately the energy scale in the plot appeared to be significantly nonlinear thus making the use of the data impractical.

The $^{23}\text{Na}(p,p_1\gamma)^{23}\text{Na}$ reaction cross section was measured in [55] using a target prepared by implantation of 20 keV sodium ions into a silicon dioxide layer created on a silicon wafer. The measurements were performed in the energy range of 1.0 – 1.7 MeV using a NaI(Tl) detector. The cross sections presented in a plot in absolute units (mb) are about 10 times greater than the data of [51]. Also the relative height of peaks is different. The energy region covered in the measurements of [51] partly overlaps with the energy range of [52] and the corresponding data sets have the same order of magnitude. This indicates that the data [55] are probably incorrect and so they were discarded in the present work.

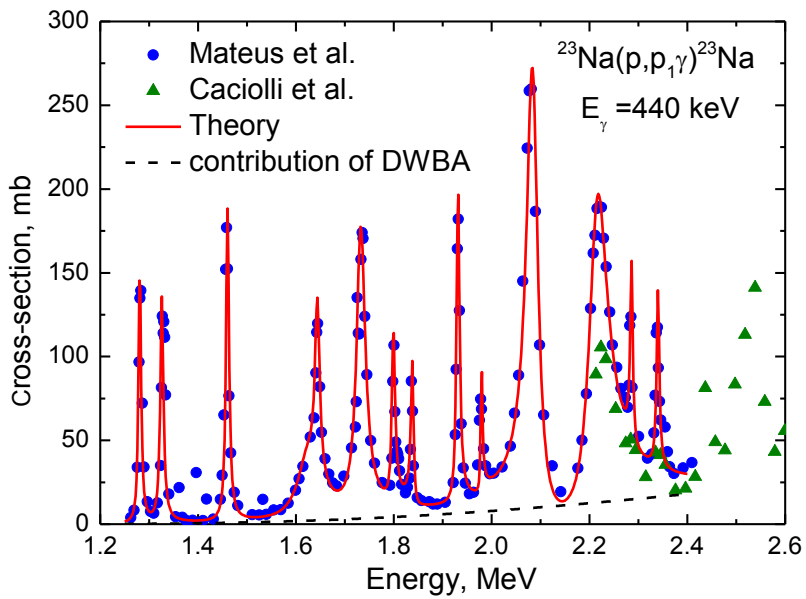


Fig. 15. Evaluated cross section and available experimental data for the 440 keV gamma ray from the $^{23}\text{Na}(p,p_1\gamma)^{23}\text{Na}$ reaction.

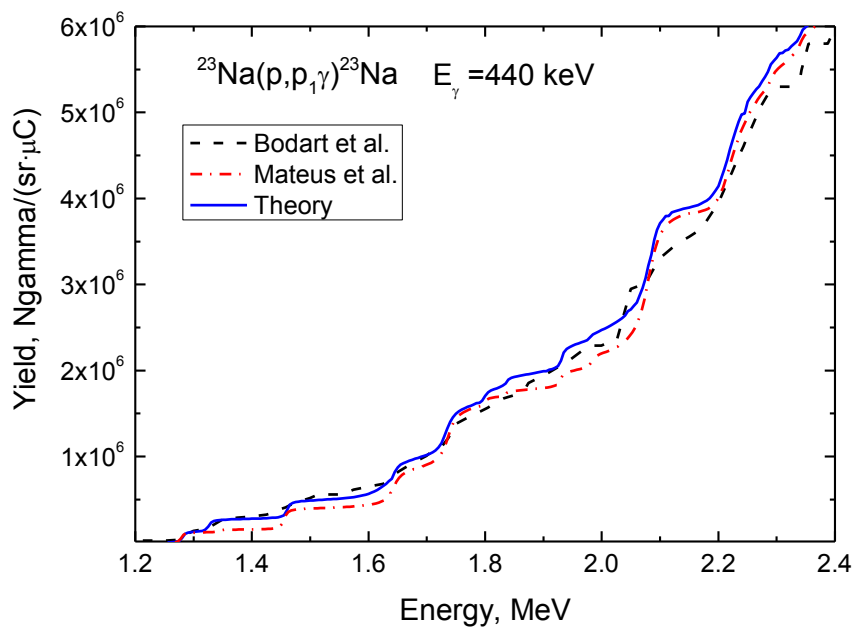


Fig. 16. Evaluated and experimental thick target gamma yield for the 440 keV gamma ray from the $^{23}\text{Na}(p,p_1\gamma)^{23}\text{Na}$ reaction.

The comparison of the data [51] and [52] shows significant discrepancy of the data sets, the structure of the cross section in [51] being much sharper. Therefore it was decided to restrict the evaluation to the energy range of the work [51]. The calculations of the resonance part of the cross section were made in the framework of the R-matrix theory. In order to find the gamma-ray production from the $^{23}\text{Na}(p,p_1\gamma)^{23}\text{Na}$ reaction the inelastic $^{23}\text{Na}(p,p_1)^{23}\text{Na}$ cross section was calculated. According to the ^{23}Na level scheme the first excited state ($J^\pi = 5/2^+$, $E_x = 440$ keV) is populated mainly directly following the proton emission. The 2nd excited state in ^{23}Na decays predominantly to the 1st one, however its energy is 2.076 MeV and in the energy range under consideration the population of this level is significantly suppressed by the Coulomb barrier. On the other hand the 1st state in ^{23}Na may also be excited through the direct process. This part of the cross section was calculated in the framework of the distorted wave Born approximation (DWBA) using the code DWUCK4 [56]. The initial data for the resonance parameters needed for the R-matrix calculations were taken from [57]. The optimization was then made using the available experimental data. The results of the cross-section calculations are presented in Fig. 15. Thick target yield was also calculated and is compared with experimental data in Fig. 16. As is seen from Fig. 15 the theoretical curve was fitted to be very close to the experimental data [51]. A few outlying experimental points around 1.4 MeV correspond to narrow resonances also observed in [54]. However, the available experimental data are insufficient for fitting and so these resonances were omitted in the calculations. Being rather narrow and weak these resonances produce an insignificant contribution to the gamma-ray yield (see Fig. 16).

2.4.2. The $^{27}\text{Al}(p,p_1\gamma)^{27}\text{Al}$ cross section

The evaluation of the $^{27}\text{Al}(p,p_1\gamma)^{27}\text{Al}$ cross section was made using experimental data obtained in the inter-laboratory experiment performed in order to assess systematic problems of experimental facilities [58]. The $^{27}\text{Al}(p,p_1\gamma)^{27}\text{Al}$, $E_\gamma = 844$ keV (isotropic line) excitation function was measured by the PIGE CRP participants from 2.5 MeV to 3 MeV at 10 keV energy steps.

In order to find a theoretical gamma-ray production from the $^{27}\text{Al}(p,p_1\gamma)^{27}\text{Al}$ reaction the inelastic (p,p') cross section was calculated in a way it was described above for the sodium case. According to the ^{27}Al level scheme the first excited state ($J^\pi = 1/2^+$, $E_x = 844$ keV) is populated mainly directly after proton emission in the energy range under consideration with ~3% transition from the second state ($J^\pi = 3/2^+$, $E_x = 1015$ keV). As the cross-section magnitudes for the $^{27}\text{Al}(p,p_1)^{27}\text{Al}$ and $^{27}\text{Al}(p,p_2)^{27}\text{Al}$ reactions are comparable both the cross sections were calculated and the contribution from the second excited state was thus taken into account. The initial data for the resonance parameters needed for the R-matrix calculations were taken from [59]. The optimization was then made using the whole set of the experimental data measured by the CRP participants. The results are presented in Fig. 17 where different sets of experimental data are marked by the laboratory representative names and an evaluated cross section is shown by a solid line. As is seen from the figure the evaluated curve provides a sort of averaging of the available experimental data. As far as this averaging is based on the physical approach it is a safe assumption that the evaluated data are more reliable than any of the individual data sets.

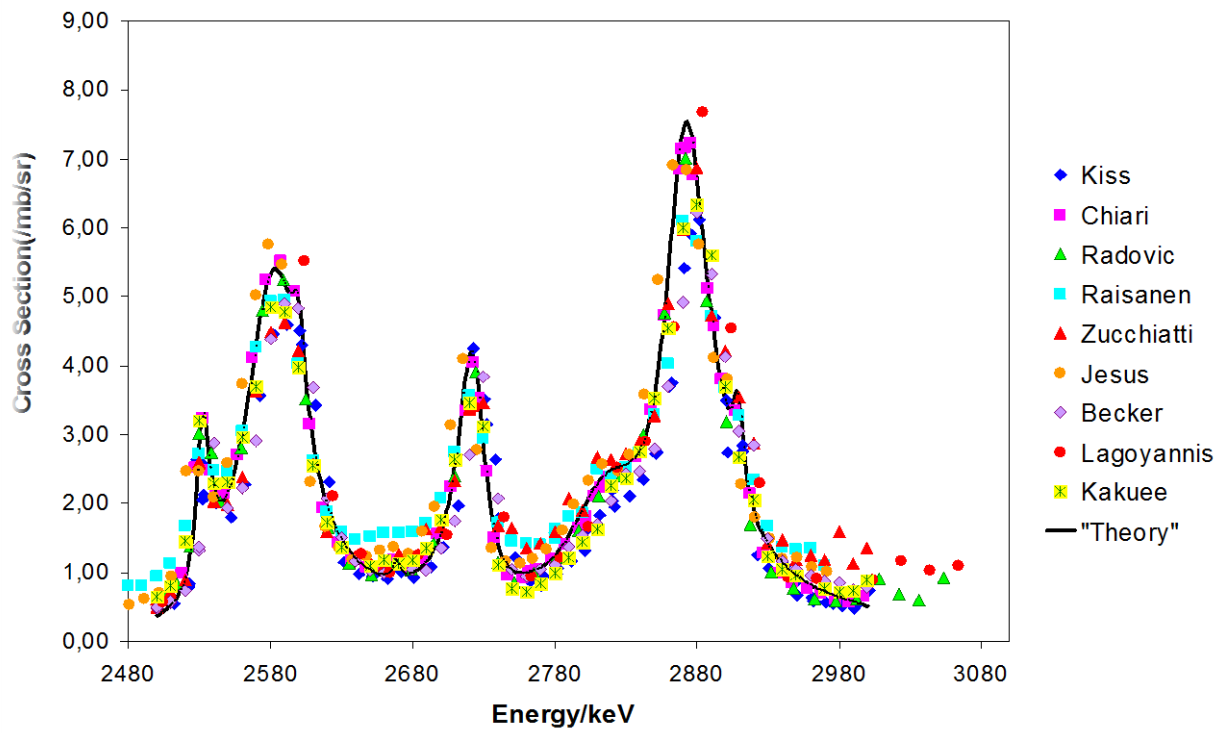


Fig. 17. Evaluation of the $^{27}\text{Al}(p,p_1\gamma)^{27}\text{Al}$ cross section.

2.4.3. The $^{52}\text{Cr}(p,\gamma)^{53}\text{Mn}$ cross section

Whereas for light nuclei the cross section has resonance structure, for heavy nuclei the level density is high, and levels overlap at relatively low excitation energy with the level widths becoming greater than the distance between levels. This results in a smoother dependence of the cross section on energy. The cross section in this energy region can be calculated in the framework of Hauser-Feshbach theory which predicts reaction cross sections averaged over many resonances in the intermediate (compound) nuclei. The reaction cross section for formation of the compound nucleus can be expressed in terms of optical model transmission coefficients. For the decay of the compound nucleus it is assumed that the reaction proceeds in a series of binary reaction stages and at each stage particle and gamma ray emission are calculated.

The $^{52}\text{Cr}(p,\gamma)^{53}\text{Mn}$ reaction was chosen for the study of the approaches to the evaluation of the data of such kind. The most prominent γ ray from $^{52}\text{Cr}(p,\gamma)^{53}\text{Mn}$ is that at 378 keV corresponding to a transition from the first excited state. This γ ray is therefore most suitable for the PIGE analysis of chromium. The available experimental information relevant to PIGE is rather scarce for medium and heavy nuclei as compared with light ones. Experimental data for this reaction cross section were found in [60]. The reported cross section was measured in the energy range 0.84 – 4.0 MeV with a Ge(Li) detector located at 55° to the beam axis.

The calculations were performed using statistical model code GNASH [61], the transmission coefficients being calculated with optical model code SCAT2 [62]. Both resolved levels and continuum were included in the statistical model calculations of the transitions leading to the population of the first excited state in the residual nucleus. The results of the calculations are presented in Fig. 18. They appeared to be rather sensitive to the optical potential which was optimized to produce the best fit to the experimental data (see Fig. 19). The sensitivity to the level density model appeared to be low (Fig. 20).

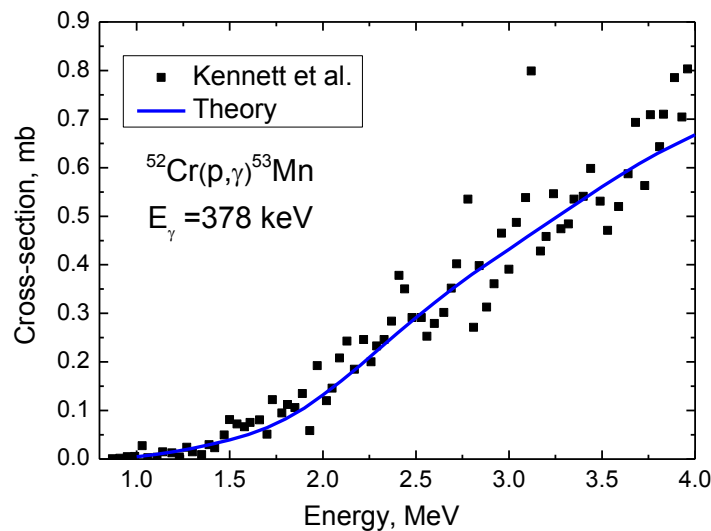


Fig. 18. Evaluated cross section and available experimental data for the 378 keV gamma ray from the $^{52}\text{Cr}(p,\gamma)^{53}\text{Cr}$ reaction.

Along with a general smooth increase on energy, some resonance structure is seen in the experimental cross section presented in Fig. 18. It corresponds to isobaric analogue resonances (IARs) caused by the population of isobaric analogue states in the compound nucleus. IARs usually have a decay scheme different from the background resonances, and unique primary gamma rays from the decay of IARs can be used for resonance profiling [63-64].

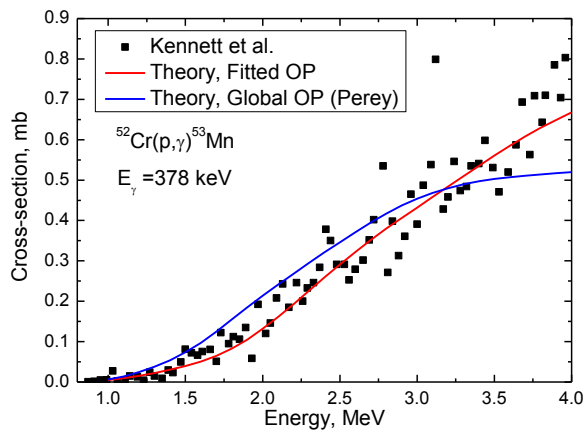


Fig. 19 Effect of the optical potential variation on the calculated cross section.

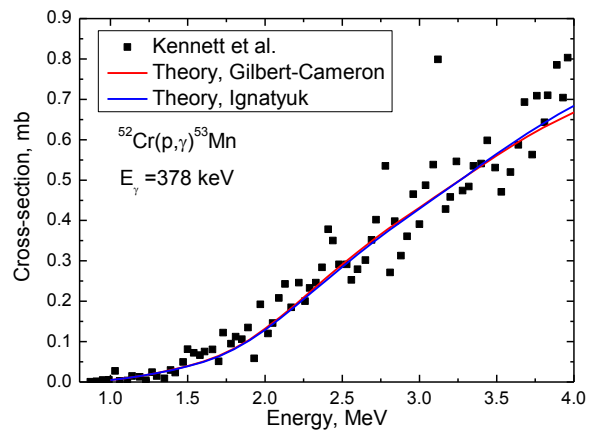


Fig. 20. Effect of the level density model on the calculated cross section.

3. Conclusions

The work performed in the framework of a CSA is as follows:

As a result of the search in the literature 34 files including 30 related to PIGE were prepared in the R33 format and submitted to NDS for uploading onto IBANDL. 27 files relevant to IBA including 10 related to PIGE were found in the EXFOR data base and their accession numbers were sent to NDS. The graph numbers from 29 references including 17 related to PIGE were sent to NDS for digitizing and preparing R33 files.

SigmaCalc was made available to the community from a different server provided by the University of Surrey and was updated with new evaluations. In order to provide the possibility to compare evaluated cross sections with corresponding experimental data an improved presentation of the data was developed including the conversion of the PIGE cross section into thick target yield on the fly. SigmaCalc now makes external calls to IBANDL to retrieve current data files. In order to provide the possibility to integrate SigmaCalc into the current IBANDL it was configured to send R33 files with results of calculations in response to the external calls.

IAEA NDS has now made available two options of evaluated SigmaCalc cross-section data from the IAEA IBANDL interface (<http://www-nds.iaea.org/ibandl/>): pre-calculated 'frozen' cross-section data obtained with SigmaCalc versions 1.6 and 2.0, and 'on-the-fly' calculations through direct calls to the University of Surrey web server.

The $^{12}\text{C}(d,p_0)^{13}\text{C}$, $^{28}\text{Si}(\alpha,\alpha_0)^{28}\text{Si}$, $^{\text{nat}}\text{Si}(\alpha,\alpha_0)^{\text{nat}}\text{Si}$, and $^{13}\text{C}(p,p_0)^{13}\text{C}$ cross sections were evaluated and benchmarked.

A methodology for the evaluation of the PIGE data was developed and its extension over all the PIGE cross sections seems to be straightforward. The evaluation was made for $^{23}\text{Na}(p,p_1\gamma)^{23}\text{Na}$, $^{27}\text{Al}(p,p_1\gamma)^{27}\text{Al}$, and $^{52}\text{Cr}(p,\gamma)^{53}\text{Mn}$ cross sections.

References

1. A newsletter of the Nuclear Data Section (NDS) No. 53, May 2012 p.1.
2. A newsletter of the Nuclear Data Section (NDS) No. 55, May 2013 p.3.
3. P. D. Kunz, G. N. Hassold, J. J. Kraushaar and P. A. Smith, *Nucl. Phys.* **A367**, 1981, p. 13-28.
4. G. D. Putt, *Nucl. Phys.* **A161**, 1971, p. 547-564.
5. G. R. Satchler, *Nucl. Phys.* **85**, 1966, p. 273-287.
6. A. Gallmann, P. Fintz, and P. E. Hodgson, *Nucl. Phys.* **82**, 1966, p. 161-181.
7. von K. Gmür and H. H. Müller, *Helv. Phys. Acta* **46**, 1974, p. 807-823.
8. A. M. Lane, R. G. Thomas, *Rev. Mod. Phys.*, **30** (1958) 257.
9. E. Kashy, R. R. Perry and J. R. Risser, *Phys. Rev.* **117** (5), 1960, p. 1209-1296.
10. V. G. Balin, A. F. Gurbich and V. S. Shorin, Preprint FEI-1341, Obninsk (1982).
11. I. Ya. Barrit+, (1986), Jour. Kratkie Soobshcheniya po Fizike, Vol.7, p.29.
12. A. P. Klyucharev et al. *Izvestiya Akademii Nauk* v.30 (1966) 224.
13. M. Huez, L. Quaglia, G. Weber, *Nucl. Instr. and Meth.* **105**, 1972, p. 197-203.
14. M. Lambert, G. Dumazet, Ch. Benedetti, D. Gresillon, *Acad. Sc. Paris* 262 (1966).
15. N. Jarmie and J. D. Seagrove, Los Alamos Report LA-2014 (1957).
16. R. A. Jarjis, *Int.Rep.*, U. of Manchester (1979).
17. V. Quillet, F. Abel, and M. Schott, *Nucl. Instr. and Meth.* **B83**, 1993, p. 47-61.
18. J. A. R. Pacheco de Carvalho, A. D. Reis, *Nucl. Instr. and Meth.* **B266**, 2008, p. 2263-2267.
19. M. T. McEllistrem, K. W. Jones, R. Chiba, R. A. Douglas, D. F. Herring, and E. A. Silverstein, *Phys. Rev.* **104** (4), 1956.
20. W. Jiang, V. Shutthanandan, S. Thevuthasan, D. E. McCready, W. J. Weber, *Nucl. Instr. and Meth.* **B222**, 2004, p. 538-546.
21. G. Debras and G. Deconninck, *J. of Radioanal. Chem.*, **38**, 1977, p. 193-204.
22. J. A. Davies and P. R. Norton, *Nucl. Instr. and Meth.* **168**, 1980, p. 611-615.
23. M. Kokkoris, P. Misaelides, S. Kossionides, Ch. Zarkadas, A. Lagoyannis, R. Vlastou, C. T. Papadopoulos, A. Kontos, *Nucl. Instr. and Meth.* **B249**, 2006.
24. W. N. Lennard, G. R. Massoumi, P. F. A. Alkemade, I. V. Mitchell, and S. Y. Tong, *Nucl. Instr. and Meth.* **B61**, 1991, p. 1-7.
25. R. B. Firestone, V. S. Shirley, C. M. Baglin, S. Y. Frank Chu, and J. Zipkin, 'Table of Isotopes', 8th Edition, Vol. 1, John Wiley & Sons, Inc., New Jersey (1996).
26. F. Ajzenberg-Selove, *Nucl. Phys.*, **A268** (1976) 1, *Nucl. Phys.*, **A523** (1991) 1.
27. D. Abriola, A.F. Gurbich, M. Kokkoris, *Nucl. Instr. and Meth.* **B301** (2013) 41.
28. K.-M. Kallman *Zeitschrift fuer Physik A, Hadrons and Nuclei*, Vol.356, p.287 (1996)
29. A. Coban, F.Z. Khiari, M.S. Abdelmonem, A. Aksoy, A.A. Naqvi *Nuclear Physics, Section A*, Vol.678, p.3 (2000).
30. J.J. Lawrie, A.A. Cowley, D.M. Whittal, S.J. Mills, W.R. McMurray *Zeitschrift fuer Physik A, Hadrons and Nuclei*, Vol.325, p.175 (1986).
31. M.K. Leung, Ph.D. dissertation, Univ. of Kentucky (1972).
32. Cheng Huan-Sheng, Shen Hao, Yang Fujia, Tang Jia-Yong *Nucl. Instrum. Methods in Physics Res., Sect. B*, Vol.85, p.47 (1994).
33. R. Somatri, J.F. Chailan, A. Chevarier, N. Chevarier, G. Ferro, Y. Monteil, H. Vincent, J. Bouix *Nucl. Instrum. Methods in Physics Res., Sect. B*, Vol.113, p.284 (1996).
34. C. Ouellet, B. Singh *Nuclear Data Sheets* 112, 2199 (2011).
35. P.M. ENDT *Nuclear Physics A* 521 (1990) 1-830.
36. K.-M. Kallman, *Zeitschrift fuer Physik A, Hadrons and Nuclei* 356, 287 (1996).
37. A. Coban, F.Z. Khiari, M.S. Abdelmonem, A. Aksoy, A.A. Naqvi, *Nuclear Physics A* 678, 3 (2000).

38. J.J. Lawrie, A.A. Cowley, D.M. Whittal, S.J. Mills, W.R. McMurray, *Zeitschrift fuer Physik A, Hadrons and Nuclei* 325, 175 (1986).
39. M.K. Leung, Ph.D. dissertation, Univ. of Kentucky (1972).
40. H.-S. Cheng, H. Shen, F. Yang, J.-Y. Tang, *Nuclear Instruments and Methods in Physics Research B* 85, 47 (1994).
41. R. Somatri, J.F. Chailan, A.Chevarier, N.Chevarier et al., *Nucl. Instrum. Methods in Physics Research B* 113, 284 (1996).
42. D. Niemann, G. Konac, S. Kalbitzer, *Nucl. Inst. Meth. Phys. Res. B* 118, 11 (1996).
43. C. Jeynes, N.P. Barradas, M.J. Blewett, R.P. Webb, *Nucl. Inst. Meth. Phys. Res. B* 136-138, 1229 (1998).
44. V.A. Latorre, J.C. Armstrong, *Jour. Physical Review* 144 (1966) 891.
45. E. Milne , *Phys. Rev.* 93 (1954) 762.
46. D.G. Gerke, D.R. Tilley, N.R. Fletcher, R.M. Williamson, *Nucl. Phys.* 75 (1966) 609.
47. D.Zipoy, G. Freier, K. Famularo, *Phys. Rev.* 106 (1957) 93.
48. H.J. Kim,W.T. Milner, F.K. McGowan, *Nuclear Data Tables v.A2* (1966) 353.
49. E. Kashy, R. R. Perry, R. L. Steele, J. R. Risser, *Phys. Rev.* 122 (1961) 884.
50. N.P. Barradas, N. Catarino, E. Alves, I. Bogdanovic Radovic, A.F. Gurbich, *Nucl. Inst. Meth. Phys. Res.B* 316 (2013) 81.
51. R. Mateus, A.P. Jesus, J. Cruz, J.P. Ribeiro, *Nucl. Instr. and Meth. B* 219–220 (2004) 307.
52. A. Caciolli, G. Calzolari, M. Chiari, A. Climent-Font, G. Garcia, F. Lucarelli, S. Nava, *Nucl. Instr. and Meth. B* 266 (2008) 1392.
53. F. Bodart, G. Deconninck, G. Demortier, *J. of Radioanal. Chem.* 35 (1977) 95.
54. M.A. Meyer, J.P.L. Reinecke, D. Reitmann, *Nucl. Phys. A* 185 (1972) 625.
55. P. Trocellier, Ch. Engelmann, *J. of Radioanal. Chem.* 67 (1981) 135.
56. P.D. Kunz, G.N. Hassold, J.J. Kraushaar, P.A. Smith, *Nucl. Phys. A* 367 (1981) 13.
57. J.R. Vanhoy, E.G. Bilpuch, C.R. Westerfeldt, G.E. Mitchell, *Phys. Rev. C* 36 (1987) 920.
58. Summary Report on the 2nd Research Coordination Meeting Development of a Reference Database for Particle-Induced Gamma ray Emission (PIGE) Spectroscopy, INDC(NDS)-0625, March 2013, IAEA, Vienna, Austria.
59. R.O. Nelson, E.G. Bilpuch, C. R. Westerfeldt, G.E. Mitchell, *Phys. Rev. C* 30 (1984) 755.
60. S.R. Kennett, L.W. Mitchell, M.R. Anderson, D.G. Sargood, *Nucl. Phys. A* 363 (1981) 233
61. P.G. Young, E.D. Arthur, M.B. Chadwick, *Comprehensive Nuclear Model Calculations: Introduction to the Theory and Use of the GNASH Code.* LA-12343-MS (July 1992).
62. O.Bersillon, *SCAT2: Un programme de modele optique spherique*, CEA-N-2227 (October 1981).
63. C.R. Gossett, *Nucl. Instr. and Meth.* 168 (1980) 217.
64. Z.E. Switkowski, R.J. Petty, J.C.P. Heggie, G.J. Clark, *Nucl. Instr. and Meth.* 159 (1979) 407.

Nuclear Data Section
International Atomic Energy Agency
Vienna International Centre, P.O. box 100
A-1400 Vienna, Austria

E-mail: nds.contact-point@iaea.org
Fax: (43-1) 26007
Telephone: (43-1) 2600 21725
Web: <http://www-nds.iaea.org>
